Conference Paper, Published Version

Ferreira, Rui; Amatruda, M.; Simão, J.; Ricardo, Ana Margarida; Franca, Mario; Di Cristo, Cristiana

Influence of bed morphology on double-averaged turbulent quantities in low submergence gravel-bed flows

River Flow 2010 - Dittrich, Koll, Aberle & Geisenhainer (eds) - © 2010 Bundesanstalt für Wasserbau ISBN 978-3-939230-00-7

Influence of bed morphology on double-averaged turbulent quantities in low submergence gravel-bed flows

Rui M.L. Ferreira, Mafalda Amatruda & Joana Simão
CEHIDRO–Instituto Superior Técnico, TULisbon, Portugal

Ana M. Ricardo
CEHIDRO-Instituto Superior Técnico, TULisbon, Portugal, and EPFL, Lausanne

Mário J. Franca
FCT–New University of Lisbon & IMAR–Centre for Marine and Envir. Research, Portugal

Cristiana Di Cristo
DiMSAT - University of Cassino, Cassino (FR) Italy

ABSTRACT: In river rehabilitation studies it is necessary to assess the impacts of the modified sand content, namely on near-bed flow hydrodynamics. This laboratory study addresses the changes that different bed morphology configurations and sediment transport impose on hydrodynamic variables relevant for the momentum and turbulent kinetic energy (TKE) budgets. Bed morphology was characterized by the void function, sand content, basal porosity and bed thickness. Special emphasis was given to the characterization of mean Reynolds and form-induced stresses, near-bed pressure, mean longitudinal velocity, momentum diffusivity and TKE production. Five laboratory tests simulated different stream conditions and sand contents in a framework-supported gravel bed. Instantaneous velocity maps were obtained with Particle Image Velocimetry (PIV). The collected data was analysed and theoretically framed with double-averaged methods (DAM). The impacts of the variations in the bed morphology over the near-bed flow hydrodynamics are discussed by direct comparison of the normalised DA flow variables. It was found that the effect of near-bed sediment movement is felt primarily in the wake production terms, in the shear rate below the plane of the crests and, to a lesser extent, in the form-induced shear stresses.

Keywords: Gravel-sand beds; Turbulent flows, Sediment transport, Double-averaged methodology, PIV

1 INTRODUCTION

In mountain rivers, the bed is generally composed of a gravel-sand mixture. The sand content may vary, changing the characteristics of the bed morphology. This may happen seasonally or a as trend, resulting from the erosion of unprotected soil in the catchment. In the latter case, the introduction of sand and sand bedload may bring about negative impacts on the reproductive cycle of salmonis and macroinvertebrate species (Kondolf 2000, Ferreira et al. 2009). When the porosity of the bed substrate becomes reduced, due to the sand matrix that forms in the otherwise open gravel framework, beyond the capacity for natural rehabilitation, intervention may be needed. In river rehabilitation studies it is thus necessary to assess the impacts of the modified sand content, namely on near-bed flow hydrodynamics, to determine the extent of the required intervention.

This study benefits from recent theoretical progress in the characterization of the 3D flow over irregular boundaries, the double avereraged methodology (DAM). This is a particular form of upscaling, in both time and space: the conservation equations of turbulent flows are expressed for time-averaged quantities which, in case of unsteady flow, are defined in a time-window smaller than the fundamental unsteady flow time-scale, and for space-averaged quantities, defined in space windows larger than the characteristic wavelength of the boundary irregularities (Smith & McLean 1977, Franca & Czernuszenko 2006, Ferreira et al. 2009). The formal apparatus of DAM has been built in the study of flows within porous media (Gray & Lee 1977), of atmospheric boundary layers to describe turbulent flows within and above terrestrial canopies (Raupach et al. 1991, Finnigan 2000), of hydraulically rough beds due to bedforms (Smith & McLean 1977, Gimenez-Curto and Corniero

Lera 1996), of sand-gravel roughness (Nikora et al. 2001, Nikora et al. 2007, Pokrajac et al. 2008, Franca et al. 2008, Ferreira et al. 2009) and of hydraulic flows over and within vegetation (Lopez and Garcia 2001).

Although this formal apparatus encompasses now statistically time-invariant mobile boundaries (Nikora et al. 2007), little work has been produced to understand the influence of bed morphology on DA flow variables.

This study addresses this need and is aimed at the characterization of the changes that different bed morphology configurations and different sand transport rates impose on hydrodynamic variables relevant for the momentum and turbulent kinetic energy (TKE) budgets. To accomplish the proposed objectives, conditions similar to those found in nature, in what concerns the flow and the characteristics of the bed material, were reproduced in the laboratory. Five experimental tests simulated different stream conditions and sand contents in a framework-supported gravel bed. Instantaneous velocity maps were obtained with Particle Image Velocimetry (PIV). The collected data was analysed and theoretically framed with DAM.

In Section 2 the main theoretical concepts are expounded. Section 3 is dedicated to the laboratory tests and to the presentation of the laboratorial facilities and instrumentation. Data collection issues are discussed in Section 4. The main results are presented and discussed in Section 5. Conclusions and recommendations close the paper.

2 CONCEPTUAL FRAMEWORK

Double-averaged Navier-Stokes equations (DANS) and double-averaged equation of conservation of TKE (DATKE) replace Reynolds-averaged Navier-Stokes (RANS) equations and time-averaged TKE conservation equations for flows over irregular rough boundaries. For steady flows, these equations are, respectively,

$$\begin{aligned}&\langle \overline{u}_i \rangle \frac{\partial \langle \overline{u}_j \rangle}{\partial x_i} = g_j - \frac{1}{\varphi \rho^{(w)}} \frac{\partial \varphi \langle \overline{p} \rangle}{\partial x_j} - \frac{1}{\varphi} \frac{\partial \varphi \langle \overline{u'_j u'_i} \rangle}{\partial x_i} \\ &- \frac{1}{\varphi} \frac{\partial \varphi \langle \widetilde{u}_j \widetilde{u}_i \rangle}{\partial x_i} + \frac{1}{\varphi} \frac{\partial}{\partial x_i} \varphi \left\langle \nu^{(w)} \frac{\partial \langle \overline{u}_j \rangle}{\partial x_i} \right\rangle \\ &+ \frac{1}{\rho^{(w)} V_f} \int_{S_{\text{int}}} \overline{p}\, n_j \, \mathrm{d}S - \frac{1}{V_f} \int_{S_{\text{int}}} \nu^{(w)} \frac{\partial \overline{u}_j}{\partial x_i} n_i \, \mathrm{d}S + \langle \overline{f}_j \rangle\end{aligned} \tag{1}$$

and

$$\begin{aligned}&- \langle \overline{u'_i u'_j} \rangle \frac{\partial \langle \overline{u}_j \rangle}{\partial x_i} - \langle \overline{u'_i u'_j} \rangle \left\langle \frac{\partial \tilde{u}_j}{\partial x_i} \right\rangle - \left\langle \widetilde{u'_i u'_j} \frac{\partial \tilde{u}_j}{\partial x_i} \right\rangle = \\ &\langle \varepsilon \rangle + \frac{1}{\varphi} \frac{\partial}{\partial x_j} \left(\varphi \langle \overline{u'_j k} \rangle + \frac{\varphi}{\rho^{(w)}} \langle \overline{u'_j p'} \rangle \right)\end{aligned} \tag{2}$$

where u_i is the fluid velocity, p stands for pressure, k is the turbulent kinetic energy per unit fluid mass, $\langle \varepsilon \rangle$ is the mean rate of pseudo-dissipation, g_j is the acceleration of gravity, φ is the void function, $\nu^{(w)}$ and $\rho^{(w)}$ are the viscosity and the density of the fluid, respectively, and $\langle \overline{f}_j \rangle$ stands for the force (per unit fluid mass) arising from the interaction between fluid and particles moving as bedload (Ferreira et al. 2008).

In equation (1), $-\rho^{(w)} \varphi \langle \overline{u'_j u'_i} \rangle$ and $-\rho^{(w)} \varphi \langle \widetilde{u}_j \widetilde{u}_i \rangle$ represent the mean Reynolds and the form-induced stress tensor and term $\rho^{(w)} \varphi \langle \nu \partial \langle \overline{u}_j \rangle / \partial x_i \rangle$ is the viscous stress tensor. Terms $1/V_f \int_{S_{\text{int}}} \overline{p}\, n_j \, \mathrm{d}S$ and $-\frac{\rho^{(w)}}{V_f} \int_{S_{\text{int}}} \nu \frac{\partial \langle \overline{u}_j \rangle}{\partial x_i} n_i \, \mathrm{d}S$ are momentum sinks; they stand for pressure and viscous drag per unit mass, respectively. Term

$$\langle \overline{f}_j \rangle \simeq \langle f_x \rangle = \frac{1}{2} C_D \int_0^{h_b} \left\langle \varphi C_b \left(\overline{u} - \overline{u_p} \right)^2 \right\rangle \mathrm{d}z \,, \tag{3}$$

where C_D is a drag coefficient, h_b is the thickness of the transport layer, C_b is the flux-averaged concentration of moving particles and up $\overline{u_p}$ is the path-averaged particle velocity, accounts for the momentum sink due to sediment transport under the hypothesis of small concentrations of sediment transported as bedload. In a steady flow under quasi-equilibrium sediment transport the fundamental term to express fluid-particle interactions should be drag on moving sediment.

In equation (2) $-\langle \overline{u'_i u'_j} \rangle \frac{\partial \langle \overline{u}_j \rangle}{\partial x_i}$ is the rate of production due to Reynolds stresses,

$$\begin{aligned}&- \langle \overline{u'_i u'_j} \rangle \left\langle \frac{\partial \tilde{u}_j}{\partial x_i} \right\rangle - \left\langle \widetilde{u'_i u'_j} \frac{\partial \tilde{u}_j}{\partial x_i} \right\rangle = \\ &- \langle \overline{u'_i u'_j} \rangle \frac{\langle \overline{u}_j \rangle}{\varphi} \frac{\partial \varphi}{\partial x_i} - \left\langle \widetilde{u'_i u'_j} \frac{\partial \tilde{u}_j}{\partial x_i} \right\rangle\end{aligned} \tag{4}$$

is the rate of production due to form-induced stresses (wake production) and

$$\frac{1}{\varphi} \frac{\partial}{\partial x_j} \left(\varphi \langle \overline{u'_j k} \rangle + \frac{\varphi}{\rho^{(w)}} \langle \overline{u'_j p'} \rangle \right)$$

is the diffusion of TKE, incorporating the gradient of the flux of TKE and pressure diffusion.

Assuming that the turbulent boundary layer is fully developed over an irregular, porous, mobile bed composed of a poorly sorted mixture of cohesionless particles in the sand-gravel range, and that the bedload discharge (and the fractional bedload discharges) are time-invariant in a domain whose longitudinal scale is several times the flow depth and no significant bed forms develop, the flow can be divided in four main regions (figure 1): the outer region (A), the inner region (B), the pythmenic region (C) and the hyporeic region (D). There is overlapping among all regions as the phenomena that characterises each region does not cease to exist abruptly. In region A the turbulent flow is influenced by the free-surface and scales with outer variables h and U, the depth-averaged velocity. The dissipation exceeds production of TKE and Reynolds stresses are dominant.

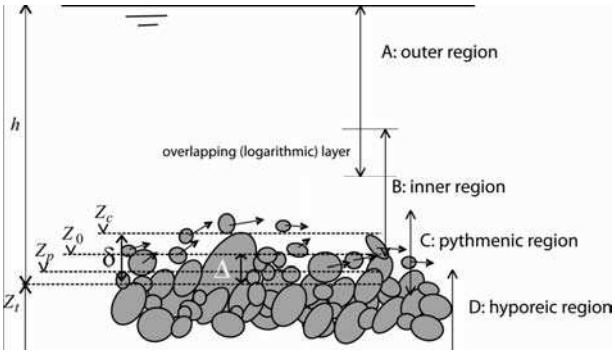

Figure 1. Idealised structure of the flow over hydraulically rough porous poorly sorted gravel-sand beds.

The flow in region B is affected by the characteristics the rough wall, directly in the lowermost layers and indirectly, through u_*, in the uppermost layers. The characteristic length scale is k_s, determined by the bed micro-topography and near-bed particle movement. In the lower layers of this region (at about the elevation of the crests) production rate is expected to exceed the dissipation rate of TKE. The lower boundary of the inner region is defined as the elevation of the zero of the log-law, Z_0, should one exist. If the relative submergence is large enough, the vertical profile of the time-averaged longitudinal velocity in the overlapping layer between the inner and outer regions is logarithmic and the production and dissipation rates should be in equilibrium (Townsend 1976). In region C, the flow is, to a great extent, determined by the bed micro-topography. Pressure and viscous drag on the immobile bed particles act as momentum sinks and become dominant toward the bottom of this region. Drag forces over moving particles constitute an extra fluid momentum sink. Form-induced stresses are relevant and should be strongly influenced by the nature of the bed. The lower boundary of the pythmenic region is Z_t. If the bed is deep, the lowermost layers of the pythmenic region do not participate in the vertical momentum exchange and Reynolds and form-induced stresses should become small compared with total (viscous and pressure) drag in the lower layers of region C and in region D.

3 FACILITIES, INSTRUMENTATION AND IDENTIFICATION OF TESTS

The experimental tests were performed in the Recirculating Tilting Flume (CRIV), of the Laboratory of Hydraulics and Environment of Instituto Superior Técnico. The CRIV is 12 m long, 0.408 m wide and has a recirculation circuit composed by four tanks, a PVC pipe system and a centrifugal pump. To feed the system with sediments, a conveyor belt was placed on the channel rails at a upstream section. The sediment discharge was controlled by the velocity of the belt and the thickness and width of the sediment streak.

Measurements of the free-surface elevation and the bed topography was done recurring to a 1 mm precision ruler and a 0.1 mm precision point gage, respectively. The void function was estimated in a bed clone in a container as the volume of water released between two consecutive water levels 2 mm apart.

Velocity measurements were performed with a PIV system composed of a double-cavity Nd:YAG SoLo laser, a CCD camera and a software-controlled acquisition system. It emits light in the green spectrum (532 nm). The light sheet is 1.5 mm thick and penetrates the flow through the free surface (details in Ferreira 2008 or Amatruda 2009).

Five laboratorial tests, S1 to S5, were performed. The flume bed is framework-supported (Hogan et al. 1999) in all three tests, i.e. the coarse-gravel elements were in contact forming a stable 3D structure whose voids were empty in test S1 (openwork gravel bed) and filled with sand, in different proportions, in tests S2 to S5. Test S1 simulated a reference situation in as much the flow in the pythmenic region is influenced only by the roughness provided by the gravel bed. In tests S2 and S4 the porosity was reduced in the substratum, influencing hydro-

dynamic conditions. For tests S3 and S5, sand content in the bed was increased until its discharge approached capacity transport rates. These tests allowed for the characterization of the impact of moving sediment over the turbulent flow in the pythmenic and interfacial layers.

The main characteristics of the tests are described next. The bed slope, i_0 = 0.00445, and the gravel framework were kept constant in all tests. The flow discharge, Q, was 23.3 ls^{-1} in tests S1 to S4 and 16.7 ls^{-1} in test S5. The gravel framework has mean diameter, $d_{50}^{(g)}$ = 28 mm, and geometric standard deviation, $\sigma_D^{(g)}$ = 1.4. The mean diameter of the sand fed into the channel is $d_{50}^{(s)} = 0.9$ mm and the geometric standard deviation, $\sigma_D^{(s)}$ is 1.6. There was no overlapping between the sand and the gravel sizes.

The bed morphology was characterized by the bed thickness, δ, the elevation of the lowest troughs, Z_t, the elevation of the highest crests, Z_c, the void function, φ and the substrate porosity, φ_0 (Table 1). The bed topography of test S1, expressed as a staggered matrix of elevation samples with a density of 1 sample/cm^2, is shown in Figure 2.

Table 1. Characterization of the bed.

Test	Z_t (m)	Z_c (m)	δ (m)	φ_0 (–)
S1	0.092	0.146	0.054	0.38
S2	0.095	0.146	0.051	0.31
S3	0.107	0.146	0.039	0.22
S4	0.091	0.144	0.054	0.35
S5	0.125	0.145	0.021	0.31

The main flow characteristics, shown in Table 2, are h, the flow depth (distance between the elevations of the troughs and of the free surface), U, the depth-averaged mean flow velocity in the longitudinal direction, u_*, the bed friction velocity, calculated 1) from the equation of conservation of momentum in the x direction, $u_* = \sqrt{gR_* i_0}$, where the hydraulic radius is $R_* = (h-\delta)0.408/(0.408+2(h-\delta))$, and 2) from total shear stress (from the total shear stress profiles) at the elevation of the crests, and $C_f = (u_*/U)^2$, the friction coefficient, calculated from definition (2) of u_*.

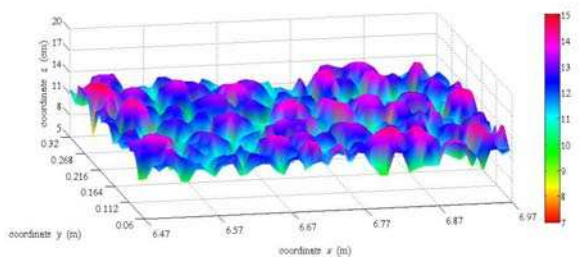

Figure 2. Bed topography of the working area.

Table 2–Mean flow parameters.

	h (m)	$u_*^{(1)}$ (ms^{-1})	$u_*^{(2)}$ (ms^{-1})	U (ms^{-1})	C_f (ms^{-1})
S1	0.161	0.056	0.052	0.426	0.0169
S2	0.156	0.058	0.055	0.438	0.0158
S3	0.127	0.052	0.046	0.532	0.0095
S4	0.163	0.056	0.050	0.419	0.0176
S5	0.107	0.051	0.033	0.595	0.0074

All flows were fully turbulent and subcritical, with Froude numbers of about 0.5.

In tests S3 and S5 sand feed was imposed until the bed was in equilibrium, *i.e.* with no visible aggradation or degradation and no bed-forms. After an iterative process, the final equilibrium discharge was $q_b = 4.77\times10^{-3}$ ls^{-1} for test S3 and $q_b = 2.08\times10^{-3}$ ls^{-1} for test S5.

4 RESULTS AND DISCUSSION

4.1 Data collection

Double-averaged quantities are defined as

$$\langle \bar{X} \rangle (z) = \frac{1}{A_f(z)} \int_{\Omega/\Sigma} \bar{X}(\alpha,\beta,z) \mathrm{d}S \qquad (5)$$

where Ω is the measuring domain. Σ is the subdomain of Ω occupied by solids, $A_f(z)$ is the area of the sub-domain, within Ω, occupied by fluid at a given elevation z. Dummy variables α and β are such that $0 < \alpha < L_x$ and $0 < \beta < L_y$ where L_x and L_y are larger than the dominant roughness wavelength.

Definition (5) is not practical when measurements are spatially discrete, for instance velocity profiles taken at a finite number of points in a given measuring area. In this latter case, the calculation of the double-averaged velocity at a given elevation z obeys

$$\langle \bar{u} \rangle (z) \approx \sum_{k=1}^{N-N_0(z)} \bar{u}_k(z) A_k(z) \Big/ \sum_{k=1}^{N-N_0(z)} A_k(z) \qquad (6)$$

where $A_k(z)$ is the area of influence of (x_k, y_k), N represents the total number of sampling

verticals and $N_0(z)$ the number of sampling points, at elevation z, for which the velocity is not defined. It should be noted that, below the crests,

$$\sum_{k=1}^{N-N_0(z)} A_k(z) < A(z) \text{ for } N_0(z) > 0 .$$

The measuring area was a rectangle of $21 \times 6\,\text{cm}^2$ (longitudinal×lateral) whose centre was at 7.3 m from the inlet. The lateral dimension is of the order of magnitude of the bed elevation fluctuation and the longitudinal dimension is one order of magnitude greater than the latter. To maintain high PIV flow resolution only the lowermost 70% of the flow depth were observed in tests S1 to S4.

The number of sampling verticals was 48, 54, 56 and 60 for S1, S2, S3 and S4 and S5, respectively with about 2000 samples for each time series. The regions of influence of each profile are the areas of the Voronoï polygons of the mesh of profiles.

4.2 Near-bed pressure distribution

In a gradually-varied flow, longitudinal gradients are small compared with vertical gradients. The flow is turbulent and, hence, viscous stresses are negligible. The vertical velocity distribution (Figure 3) is small throughout the water column.

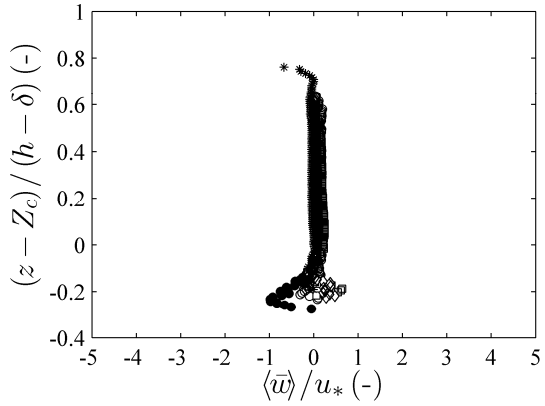

Figure 3. Non-dimensional double-averaged mean vertical velocity. Open circles (○) stand for the reference bed (S1), open squares (□) stand for S2, full circles (●) stand for S3 (mobile bed), diamonds (◊) stand for S4 and asterisks (∗) stand for S5 (mobile).

The vertical convective acceleration is about 0.3 ms^{-2}, considerably smaller than the acceleration of gravity. Hence, the main deviations from the hydrostatic pressure distribution are due no normal form-induced and Reynolds stresses.

Figure 4 shows that DA normal vertical Reynolds stresses appear to slightly decrease in the upper regions of the pythmenic region due to sediment transport; conversely (at least in test S4), vertical Reynolds stresses increase with sediment transport in the lower layers of the pythmenic region. Figure 5 shows that normal vertical form-induced stresses are essentially not influenced by sediment movement in the near bed region.

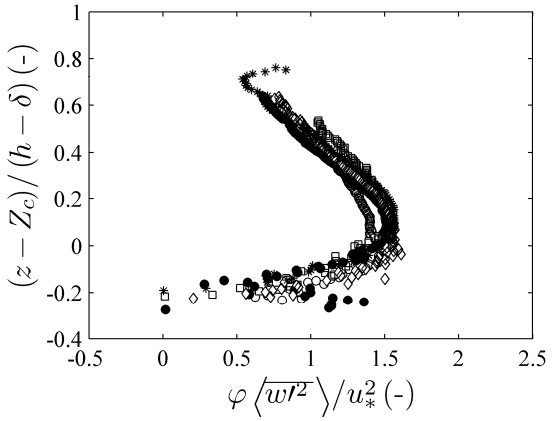

Figure 4. Non-dimensional double-averaged Reynolds vertical normal stresses. Symbols as in Figure 3.

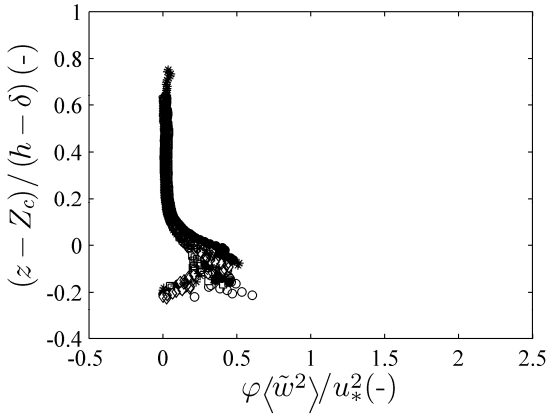

Figure 5. Non-dimensional form-induced vertical normal stresses. Symbols as in Figure 3.

Overall there should be no effect on the vertical pressure distribution since vertical gradients of these stresses are small and, at best, of second order, compared with the hydrostatic term.

4.3 Longitudinal velocity

In open-channel flow over hydraulically rough beds with large enough relative submergence, the longitudinal velocity profile in the form of

$$\frac{\langle \bar{u} \rangle}{u_*} = \frac{1}{\kappa} \ln\left(\frac{z - \Delta}{k_{sT} - \Delta} \right) + \frac{\langle \bar{u} \rangle_I}{u_*}, \qquad (7)$$

where k_{sT} is of the order of magnitude of the thickness of the pythmenic region (Figure 1), Δ is the displacement height , $\langle \bar{u} \rangle_I$ is the velocity at the top of the interfacial layer and $\kappa = 0.405$ is the von Kármán constant, may be fitted to logarithmic law above the roughness-influenced layer (Dittrich and Koll 1997, Nikora et al. 2007).

For rough mobile beds, Ferreira et al. (2008) noted that the parameters of the log-law change with the increase of bed mobility resulting in non self-similar profiles for higher transport rates.

Figure 6 shows the longitudinal velocity profile. The relative submergence is too low to guarantee complete similarity to inner and outer parameters and, hence, to guarantee a logarithmic profile (Flack et al. 2007 proposes $h/\delta > 40$). However, a log-law can indeed be fitted to the measured velocity profiles, provided that k_{sT} and $\langle\overline{u}\rangle_I$ were adequately chosen.

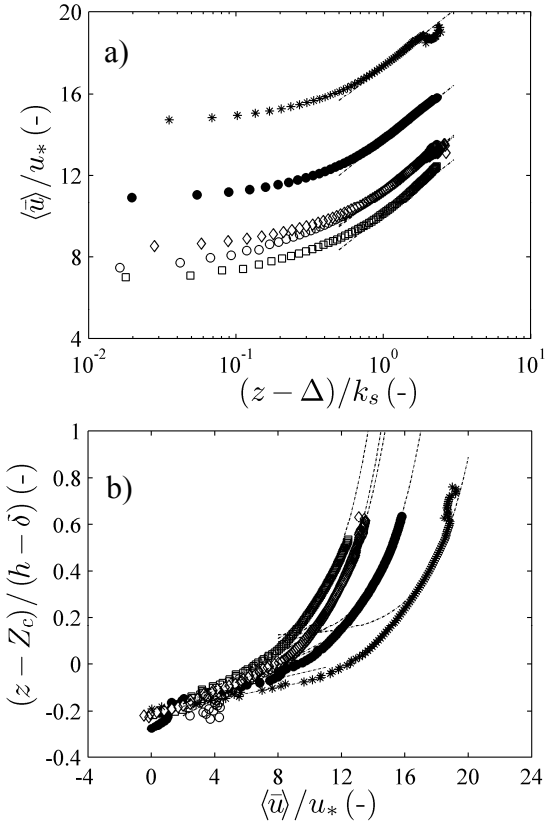

Figure 6. Double-averaged mean longitudinal velocity profiles. a) Logarithmic plot showing theoretical log-law; b) Full profile showing logarithmic and bi-lineal reaches. Symbols as in Figure 3.

Figure 6 shows also that the velocity profile in the pythmenic region can be expressed by a bi-linear law, i.e. two linear reaches with different slopes. The profiles of tests S3 and S5, influenced by sediment transport, show a higher slope of the lower linear reach. This higher shear rate is related to the lower flow resistance observed in these tests, expressed by smaller values of the friction coefficient (Table 2). This effect is mainly due to bed smoothening: the roughness elements become immersed in a layer of moving sand and, as a result, the thickness of the bed decreases. Therefore, viscous and pressure drag decrease because the total area of fluid-solid interface decreases. Drag on moving sand particles is, due to the small concentration of moving particles, not enough to raise the values of the bed shear stress.

The interaction force between moving sediment and fluid (equation 3) is an extra sink in the momentum equation. This is consistent with the finding that the total drag force *per* unit volume acting on the bed actually increases in the mobile bed cases.

4.4 Reynolds and form-induced shear stresses

Figures 7 and 8 show mean Reynolds shear stresses and form-induced shear stresses.

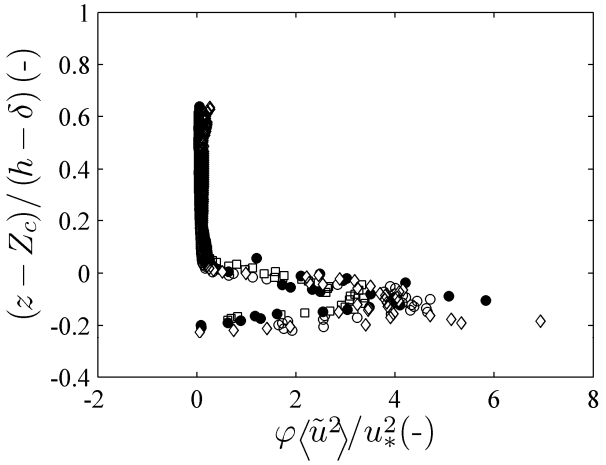

Figure 7. Non-dimensional double-averaged Reynolds shear stresses. Symbols as in Figure 3.

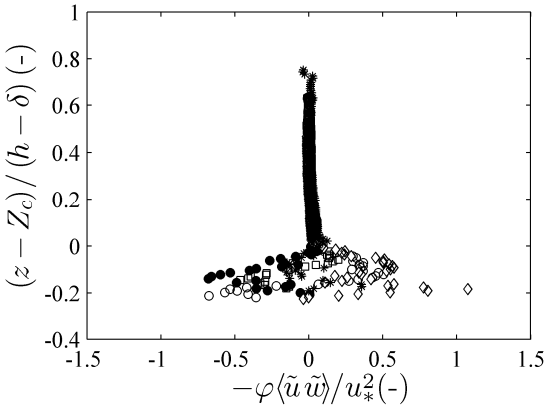

Figure 8. Non-dimensional form-induced shear stresses. Symbols as in Figure 3.

Mean Reynolds shear stresses seem unaffected by sediment transport (Figure 7). Considering the drag force on near-bed moving particles a sink in the equation of momentum in the longitudinal direction and that mean Reynolds stresses are unaffected by sediment transport, it is concluded that drag on moving particles affects form-induced stresses and on form drag. As seen in Figure 8, the profile of form-induced shear stresses is showing, in general, an alternation between positive a negative maxima in the

pythmenic region. The maxima attained in S1, the reference situation, just below the crests of the bed particles, seems attenuated in the mobile bed tests, which is consistent with an increase of drag associated to moving sediment.

4.5 Form-induced *longitudinal* normal stresses

Figure 9 shows that the longitudinal normal form-induced stresses are not significantly affected by sediment transport. The large peak exhibited in test S4 seems slightly attenuated in the remaining tests, with no special trend due to near-bed sand movement.

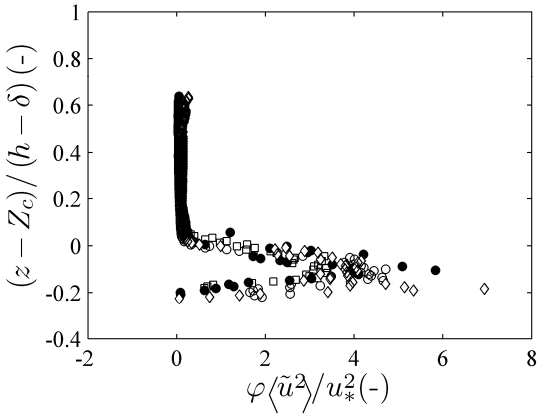

Figure 9. Non-dimensional form-induced longitudinal normal stresses. Symbols as in Figure 3.

4.6 Production *of* TKE

Figures 10 and 11 show the rate of production of TKE due to Reynolds stresses (P_r) and due to the complex flow in the wakes of the roughness elements (P_w). Considering that the flow is essentially 2DV, that the longitudinal gradients are small and taking into consideration the orders of magnitude of the remaining variables, the following simplified formulas were used

$$P_r = -\left\langle \overline{u'_j\, w'} \right\rangle \frac{\partial \left\langle \overline{u}_j \right\rangle}{\partial z} \tag{8}$$

and

$$P_w = -\left\langle \overline{u'_j\, w} \right\rangle \frac{\left\langle \overline{u}_j \right\rangle}{\varphi} \frac{\partial \varphi}{\partial z} \ . \tag{9}$$

Figure 10 shows that P_r peaks at the elevation of the crests and is fairly independent from the shape of the boundary above the crests of the bed particles. Below these crests, the scatter is considerable but there is a trend, followed in all tests, of decreasing P_r. The largest value of P_r is attained in the mobile bed tests, which is surely related to the higher shear rates exhibited by the mobile bed tests.

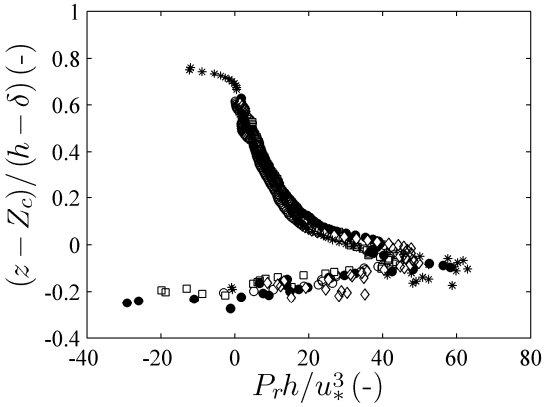

Figure 10. Rate of production of TKE associated to Reynolds stresses. Symbols as in Figure 3.

Figure 11 shows that wake production is confined to the pythmenic region. The values of P_w are markedly smaller that those of P_r. However, in the reference situation, test S1, the values of P_w are not negligible. The effect of the sediment transport on the production terms seems to be a clear attenuation of the wake production and the development of negative production due to positive form-induced stresses.

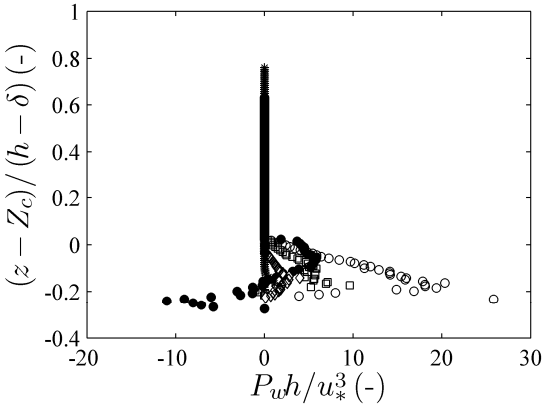

Figure 11. Rate of wake production of TKE. Symbols as in Figure 3.

5 CONCLUSION

The main results of this study may be summarized as follows.

- For the sediment concentrations assessed, there were no important impacts on the vertical pressure distribution.
- The friction coefficient is reduced in the mobile bed case. This effect should be mainly due to bed smoothening after sand introduction.

- The profile of the mean longitudinal velocity can be expressed by a log-law above the roughness-influenced layer, although the relative submersion is only moderate. One of the effects of sand transport is rendering the velocity profiles non-self-similar.
- The longitudinal velocity profile in the pythmenic region seems to be double-linear. The main effect of the sand transport is the increase of the slope in the lower linear reach.
- Viscous and pressure drag decrease in the mobile bed cases; drag on moving sand particles is not enough to increase the values of the bed shear stress.
- Mean Reynolds stresses, both shear and normal, seem unaffected by sediment transport.
- Just below the particle crests, form-induced shear stresses are smaller when the bed undergoes sediment transport. Further below there is no appreciable trend.
- The rate of production of TKE due to Reynolds stresses, P_r, peaks at the elevation of the crests and deceases below these.
- The wake production, P_w, is considerably smaller than P_r and confined to the pythmenic region. P_w is not negligible in the open-work gravel.
- The main effect of the sediment transport on the production terms seems to be a clear attenuation of the wake production and and the development of a region of negative production.

ACKNOWLEDGEMENTS

The authors acknowledge the financial support of the Portuguese Science and Technology Foundation (PTDC/ECM/65442/2006).

REFERENCES

Amatruda, M (2009). Characterization of the turbulent flow in rough-bedded open-chanel flows. Influence of the sediment discharge. MSc thesis. University Federico II.

Dittrich, A. and Koll, K. (1997). Velocity field and resistance of flow over rough surface with large and small relative submergence. Int. J. Sediment Res.: Vol. 12, No.3, pp. 21-33.

Ferreira, L (2008). Impact of Sediment Overfeeding in Gravel-Bedded River's Salmonid Habitats. MSc thesis. Instituto Superior Técnico, TU Lisbon.

Ferreira, R.M.L.; Franca, M.J.; Leal, J.G.A.B. (2008) Flow resistance in open-channel flows with mobile hydraulically rough beds. River Flow 2008 Altinakar et al. (eds). Vol. 1, pp. 385-394.

Ferreira, R.M.L.; Ferreira, L.; Ricardo, A. M. & Franca, M.J. (2009) Imposed sand transport on gravel-bedded streams. Impacts on flow variables and consequences for salmonid spawning sites. River Research and Applications, 25(10) DOI 10.1002/rra.1307.

Finnigan, J.J. 2000. Turbulence in plant canopies. Annual Review of Fluid Mechanics 32, 519–571.

Flack, K.A., Schultz, M.P., & Connelly, J.S., (2007) Examination of a Critical Roughness Height for Boundary Layer Similarity. Physics of Fluids, Vol. 19, 095104, 2007.

Franca, M.J., Ferreira, R.M.L. & Lemmin, U. (2008). Parameterization of the logarithmic layer of double-averaged streamwise velocity profiles in gravel-bed river flows. Adv. in Water Resour. 31(6): 915-925.

Franca M.J. & Czernuszenko W. (2006). Equivalent velocity profile for turbulent flows over gravel riverbeds, in River Flow 2006, R.M.L. Ferreira et al (eds) Taylor & Francis Ltd (ISBN 0415408156).

Gimenez-Curto, L.A., Corniero-Lera, M.A. 1996. Oscillating turbulent flow over very rough surfaces. J. Geophys. Res., 101(C9):20745–20758.

Gray, W.G. & Lee, P.C.Y. 1977. On the theorems for local volume averaging of multiphase systems. Int. J. Multiphase Flow, 3: 333-340.

Hogan, D.L.; Bird, S.A. & Hassan M.A. 1999. Spatial and temporal evolution of small coastal gravel-bed streams: influence of forest management on channel morphology and fish habitats in gravel-bed rivers in the environment. In: C. Klingeman, R.L. Beschta and P.D. Komar, (Eds), Water Resources Publications.

Kondolf, G.M. 2000. Assessing Salmonid Spawning Gravel Quality. Transactions of the American Fisheries Society, 129(8): 262-281.

Lopez, F., Garcia, M.H. 2001. Mean flow and turbulence structure of open-channel flow through emergent vegetation. J. Hydraul. Eng., 127(5), 392-402.

Nikora, V.; Goring, D. McEwan & I. Griffiths, G. (2001). Spatially Averaged Open-Channel Flow over Rough Bed. J. of Hydraul. Eng. 127(2):123-133.

Nikora, V., McEwan, I., McLean, S., Coleman, S., Pokrajac, D., Walters, R. 2007. Double-averaging concepts for rough-bed open-channel and overland flows: Theoretical background. J. of Hydraul. Eng. 133(8):873–883.

Pokrajac, D., McEwan, I., Nikora, V. 2008. Spatially averaged turbulent stress and its partitioning. Exp. Fluids 45:73–83.

Raupach, M.R., Antonia, R.A., Rajagopalan, S. 1991. Rough-wall turbulent boundary layers. Appl. Mech. Rev. 44(1):1–25

Smith, J.D. & McLean, S.R. (1977) Spatially averaged flow over a wavy surface. J. Geophys. Res. 83(12):1735-1746.

Townsend, A. A. (1976). The structure of Turbulent Shear Flows. 2nd Edition. Cambridge University.